Characterization of biofoulants illustrates different membrane fouling mechanisms for aerobic and anaerobic membrane bioreactors

Yanghui Xiong [1], Moustapha Harb [1], Pei-Ying Hong [1*]

[1] Water Desalination and Reuse Center, Division of Biological and Environmental Science and Engineering, King Abdullah University of Science and Technology (KAUST)

4700 King Abdullah Boulevard, Thuwal 23955-6900, Saudi Arabia

* Corresponding author:

Pei-Ying Hong

Email: peiying.hong@kaust.edu.sa

Phone: +966-12-8082218

Abstract

This study compares the membrane fouling mechanisms of aerobic (AeMBR) and anaerobic membrane bioreactors (AnMBR) of the same reactor configuration at similar operating conditions. Although both the AeMBR and AnMBR achieved more than 90% COD removal efficiency, the fouling mechanisms were different. Molecular weight (MW) fingerprint profiles showed that a majority of fragments in anaerobic soluble microbial products (SMP) were retained by the membrane and some fragments were present in both SMP and in soluble extracellular polymeric substances (EPS), suggesting that the physical retention of SMP components contributed to the AnMBR membrane fouling. One of the dominant fragments was comprised of glycoliproprotein (size 630-640 kD) and correlated in abundance in AnMBR-EPS with the extent of anaerobic membrane fouling. In contrast, all detected AeMBR-SMP fragments permeated through the membrane. Aerobic SMP and soluble EPS also showed very different fingerprinting profiles. A large amount of adenosine triphosphate was present in the AeMBR-EPS, suggesting that microbial activity arising from certain bacterial populations, such as unclassified Comamonadaceae and unclassified Chitinophagaceae, may play a role in aerobic membrane fouling. This study underlines the differences in fouling mechanisms between AeMBR and AnMBR systems and can be applied to facilitate the development of appropriate fouling control strategies.

Keywords: membrane fouling; molecular weight of biopolymers; soluble microbial product; extracellular polymeric substances; microbial community

1. Introduction

The membrane bioreactor (MBR) is a treatment process that couples membrane separation to the biological process for solid-liquid separation of the mixed liquor [1]. The integration of a membrane filtration unit achieves better effluent quality and de-couples the sludge retention time (SRT) from the hydraulic retention time (HRT) of the reactor, enabling higher biological oxygen demand (BOD) and chemical oxygen demand (COD) removal efficiency as compared to conventional activated sludge systems [2]. The MBR system can be applied to both aerobic (AeMBR) and anaerobic (AnMBR) treatment processes. Unlike the AeMBR, which has already found widespread application in low to medium strength municipal wastewater treatment [3], AnMBRs have been considered impractical for similar applications due to the perception that comparable transmembrane flux rates are not achievable. Nonetheless, the AnMBR has continued to gain consideration as an alternative treatment technology for municipal wastewater due to its potential advantages in reduced energy input, energy generation by methane production, and low sludge production [4-7].

Despite each MBR type's potential advantages, membrane fouling remains the major obstacle hindering their extensive application. It has been reported that the primary contributor to membrane pore blockage in MBRs is the deposition of the dissolved fraction of activated sludge [8, 9]. This form of less-reversible membrane fouling can lead to more rigorous forms of membrane maintenance (e.g. chemical cleaning, backwashing and high cross-flow) being necessary, diminishing the economic viability of operating MBRs for municipal wastewater treatment.

The MBR, being a biological treatment process, contains microbial cells as part of the activated sludge that produces soluble microbial products (SMP) and extracellular polymeric substances (EPS). SMP was defined by Namkung and Rittmann as being comprised of utilization-associated SMP (i.e., UAP) and biomass-associated SMP (i.e., BAP) [10]. On the other hand, EPS is comprised of a matrix of polysaccharides, proteins and other macromolecules, which collectively provide adhesion, aggregation and stabilization functions for microorganisms on a membrane surface [11]. A unified theory put forward by Laspidou and Rittmann further stated that the soluble fraction of EPS is actually SMP [12]. Based on these technical definitions of SMP and EPS, much of the existing research has focused on quantification of SMP and EPS components (e.g. proteins, polysaccharides, nucleic acids and so on) and abundance ratios between those individual components in their soluble phase [13-17]. Along with the organic matter from influent wastewater, these non-settleable organic components are one of the primary culprits inhibiting MBR performance based on their role as biofoulants [15, 18, 19].

Most of the studies that focus on elucidating the role of the soluble components of EPS and SMP on membrane biofouling were carried out in AeMBRs [15, 18-20]. Little is known about the differences between AeMBR and AnMBR fouling mechanisms as there have not been any studies that have specifically examined soluble foulants in both systems under the same operating conditions. Instead, it has conventionally being presumed that the fouling mechanisms between aerobic and anaerobic systems are similar and that most of the knowledge related to the fouling mechanisms in AeMBR systems can be extrapolated to the AnMBR [21].

Furthermore, no significant attempts have been made in previous studies to investigate the specific bacterial populations present on MBR membrane foulant layers and their correlation with the occurrence of specific soluble biofoulants contributing to membrane fouling.

In this study, it is hypothesized that AeMBRs and AnMBRs may be subject to different fouling mechanisms arising from the differences in the soluble foulant components generated by the microbial communities of both systems. To address this hypothesis, an AeMBR and AnMBR were operated using a similar reactor configuration that combined an upflow attached-growth (UA) reactor with three-successive PVDF membrane filtration units that were operated for varying time periods of up to 9 weeks to reflect different extents of membrane fouling. Quantification of the protein and carbohydrate concentrations was coupled with high performance size exclusion chromatography to determine the molecular weight distributions of proteins and polysaccharides in SMP in the permeate and retentate streams of both the AeMBR and AnMBR. The same quantification procedure was also performed on the soluble EPS from biomass attached on both aerobic and anaerobic membranes. Specific microbial populations that correlated with the extent of membrane fouling and the biofoulants were further examined using high-throughput sequencing, and their bioactivity levels evaluated by measuring adenosine triphosphate (ATP) and quorum-sensing signal molecule concentrations. Ultimately, this study aims to provide a direct multifaceted comparison of the differences in biofouling mechanisms between AeMBR and AnMBR systems.

2. Materials and methods

2.1. Reactor configuration and operating conditions

To facilitate the comparison of aerobic and anaerobic systems, the same upflow-attached (UA) reactor configuration was applied to both AeMBR and AnMBR systems (Figure 1). This reactor configuration was evaluated in this study as it was previously found to have a positive role in controlling membrane fouling in MBRs [22]. Both UA reactors were filled with ceramic ring media with an average 1.5 cm diameter and length. The seed sludge in both systems originated from the same source, and comprised of camel manure and anaerobic sludge from a wastewater treatment plant in Riyadh, Saudi Arabia [23]. No oxygen or air supply was provided in the AnMBR. Aeration was supplied to the AeMBR by two air diffusion stones at the bottom of the reactor to achieve more than 2 mg/L O_2 throughout the AeMBR system. Both reactors were fed with a synthetic wastewater of 750 mg/L carbon oxygen demand (COD) [24], and operated at 35 °C and pH of 7. Hydraulic retention times (HRTs) of both reactors were 18.5 h.

Prior to connection with membrane separation units, both UA reactors were at steady-state operation and stable performance conditions. The UA reactors were individually connected to three PVDF microfiltration (MF) membrane modules in external cross-flow mode. Membrane modules were connected in series along the recirculation line with a recirculation to effluent flow ratio of 500:1. The MF membranes were JX model MF PVDF (GE Osmonics, Minnetonka, MN, USA) and had a nominal pore size of 0.3 μm. Constant flux was maintained at 6 to 8 L/m^2/h (LMH) while changes in transmembrane pressure (TMP) were recorded by a pressure

149 gauge connected to each membrane unit. There was no sludge wasted in the anaerobic
150 system, while 150 mL of sludge suspension was taken from the aerobic reactor per
151 day, resulting in a sludge retention time (SRT) of 13 days. This was done to maintain
152 a MLSS level comparable to that in the anaerobic MBR.

153 **2.2. Soluble microbial products (SMP) and soluble extracellular polymeric**
154 **substances (EPS) sampling procedure**

155 Permeate from each membrane cassette as well as the retentate in both
156 systems were sampled weekly throughout the course of the experiment, and were
157 collectively referred to as soluble microbial products (SMP) in this study. All SMP
158 samples were centrifuged at 9,400 g for 10-30 min. The supernatant was filtered with
159 a 0.2 μm cellulose acetate membrane and stored at -20 °C prior to analyses. Analyses
160 for SMP included determination of COD, protein and carbohydrate concentrations
161 and the corresponding fingerprinting profiles of proteins and carbohydrates based on
162 molecular weight (MW) fragments. Membranes were harvested from the AeMBR at
163 time intervals of 3, 4 and 5 weeks. Membranes were harvested from the AnMBR at
164 time intervals of 3, 6 and 9 weeks. The sampling intervals were decided based on the
165 measured TMP and chosen to represent different extents of fouling on the membranes
166 (Figure 2). To harvest the membrane at each time point, one of membrane cassettes
167 was removed from the successive filtration unit, and replaced with a new membrane
168 module to ensure constant operating conditions throughout the system. Each
169 harvested membrane with an area of 20 cm by 2.5 cm was sectioned into three equal
170 parts, namely inlet, mid and outlet, based on the flow direction of the wastewater
171 stream. Soluble EPS was extracted from each section as follows: the membrane with

an area of 4 cm by 2.5 cm was cut into small strips and dispersed into two 2mL microcentrifuge tubes. 2 mL 1X PBS was added into each tube. The tubes were ultrasonicated by a QSonica Q500 Sonicator (QSonica LLC, Newton, CT, USA) for 5 min at 25% amplitude and with 2 s pulsating intervals. The membrane strips were then removed and the remaining suspension centrifuged at 9,400 g for 30 min. The supernatant after centrifugation was recovered, filtered with 0.2 μm cellulose acetate membranes and stored at -20 °C prior to analyses. The cell pellet obtained after centrifugation was also stored for DNA extraction and molecular analyses.

2.3. Protein, carbohydrate and COD quantification

Total carbohydrate concentration in the SMP and soluble EPS was determined by the phenol-sulfuric acid method with glucose as standard [25], measured in duplicate. Since the method cannot differentiate between the varying types of carbohydrates (e.g. polysaccharides, oligosaccharides and so on), measurements obtained from this method are subsequently referred to as carbohydrate concentrations in this study. Total protein concentration in the SMP and soluble EPS were detected using a protein kit from Sigma-Aldrich (TP0300, Sigma-Aldrich) with Bovine Serum Albumin (BSA) as standard and measured in triplicate. COD from all MBR reactor feeds, retentates, and permeates was determined by a HACH DR2800 Spectrophotometer (Hach, Loveland, Colorado, USA). Prior to determination of COD, the COD sample was digested via either HACH LCK 314 (15-150 mg/L) or LCK 514 COD (100-2000 mg/L) cuvette test vials (Hach-Lange, Manchester, UK) depending on the concentration to be measured.

194 **2.4. Molecular weight (MW)-based fragment analysis of proteins and**
195 **carbohydrates in SMP and soluble EPS**

196 High Performance Liquid-Size Exclusion Chromatography (HPL-SEC) was
197 employed to perform a MW-based fragment analysis of proteins and carbohydrates
198 within the SMP and soluble EPS of both AeMBR and AnMBR systems. A Waters
199 Breeze TM 2 HPLC System (Waters Chromatography, Milford, MA, USA)
200 composed of Binary HPLC pump (Waters 1525), auto sampler (Waters 2707) and
201 UV/Visible Detector (Waters 2489) was applied to separate the proteins in SMP and
202 EPS. 20 μL of each sample was injected for fragment separation on a Shodex KW-
203 802.5 column (Showa Denka America, NY) at a 20 min retention time. The mobile
204 phase was composed of 50 mM phosphate buffer with 300 mM NaCl (pH = 7.0). All
205 samples were detected with a mobile phase flow of 1 mL/min at room temperature.
206 Bigger MW fragments have a shorter retention times than those with smaller MW,
207 hence achieving fragment separation on the HPLC chromatogram. A UV detector at
208 280 nm was employed to detect the protein components [26]. The size calibration
209 standard curve of log (MW) = - (Retention Time) * 0.4483 + 8.294 (R^2 = 0.995) was
210 generated by a series of protein standards of various MW (i.e., 1.3 kDa, 6.5 kDa, 12.4
211 kDa, 29 kDa, 66 kDa, 150 kDa, 200 kDa, 443 kDa, 669 kDa) and their respective
212 retention times. A 1200 Series GPC-SEC Agilent HPLC separation system with a
213 Refractive Index Detector (RID) was applied for monitoring the MW fingerprints of
214 carbohydrates. The RID was heated to 35 °C prior to connection with the HPLC-SEC
215 system. All other operational parameters were same as those used for protein
216 separation with the exception of the mobile phase. Deionized water was used as

mobile phase as the RID detection exhibited high background noise signal when phosphate saline solution was used. The size calibration standard curve of log (MW) = -0.4786 * (Retention Time) + 8.003, with R^2 = 0.993, was generated by a series of Pullulan standards of various MW (i.e., 324, 1320, 6000, 21700, 48800, 113000, 210000, 366000, 708000 Dalton) and their respective retention times. Prior to performing MW size distribution of carbohydrates, the extracted sample in PBS was dialyzed with regenerated cellulose dialysis tubing of 3500 kDa molecular weight cut-off (Thermo Fisher Scientific, Waltham, MA, USA). The dialyzed soluble EPS was then analyzed based on above-mentioned procedure to examine the HPLC fingerprinting profiles of carbohydrates in soluble EPS.

2.5. Peptide sequencing of a protein fragment in AnMBR-EPS

The 633 kDa protein fragment within the soluble EPS of anaerobic membranes was further separated from other fragments for protein sequencing. The protein fragment was first separated by an Agilent 1260 Infinity Preparative Scale Purification System (Agilent Technologies, Santa Clara, CA, USA) equipped with a UV detector. The fragment was detected at an excitation wavelength of 280 nm, and was fractionated at 5-6 min retention time for every 50 μL of injected sample. Sufficient amount of the protein fragment was obtained after repeating the entire HPLC-based purification procedure more than 10 times. The eluted fragment was then dialyzed with regenerated cellulose dialysis tubing of 3500 kDa molecular weight cut-off (Thermo Fisher Scientific, Waltham, MA, USA). After four repeats of dialysis with deionized water, the sample was freeze-dried, and then submitted to KAUST Proteomics Core lab for protein digestion and peptide sequencing.

240 **2.6. Adenosine triphosphate (ATP) and autoinducer-2 (AI-2) quantification**

241 Bioactivity on the membranes was measured based on ATP and AI-2
242 concentrations. Adenosine triphosphate (ATP) is considered to have a core role in
243 respiration and metabolism, and is the most important energy supplier in many
244 enzymatic reactions [27]. Similarly, autoinducer-2 (AI-2) is a furanosyl borate
245 diester signal molecule secreted and responded to by many Gram-negative and Gram-
246 positive bacteria [28] during biofilm development [29, 30].

247 ATP was extracted from a 0.5 cm by 2.5 cm membrane segment. The
248 membrane was placed into a microcentrifuge tube containing 2 mL of deionized
249 water, and ultrasonicated for 1 min at 25% amplitude. After a brief vortex, the
250 membrane was removed from the tube, and the suspension was further ultrasonicated
251 for 1 to 2 min. ATP content in the suspension was quantified with the Celsis
252 amplified-ATP reagent kit on an Advance luminometer (Celsis, Westminster,
253 London, UK) with deionized water as a negative control. All samples were measured
254 in triplicate.

255 The concentration of AI-2 present in the biocake from the harvested
256 membranes was estimated by a protocol previously described [31]. Briefly, the AI-2
257 indicator *Vibrio harveyi* ATCC® strain BB170 grew overnight with autoinducer
258 bioassay (AB) medium. After overnight growth, the AI-2 culture was diluted 1:5000
259 with fresh AB medium. 20 μL of extracted soluble EPS to be tested was placed into
260 96-well solid white microplate prior to addition of 180 μL of diluted AI-2 reporter.
261 The 96-well plate containing the samples was incubated in dark on a 150 rpm shaker
262 incubator platform at 30 °C. The bioluminescent intensity was detected with the

263 Infinite M200 PRO microplate reader over time (Tecan, Männedorf, Switzerland).
264 Sterile 1X PBS that was used to extract for the soluble EPS from membranes was also
265 measured as a negative control. Varying concentrations of (S)-4,5-dihydroxy-2,3-
266 pentanedione (DPD) (Omm Scientific, Dallas, TX, USA) diluted in deionized water
267 were used as standard. The bioluminescent intensities from the samples, standards
268 and negative control increased with incubation. However, the increment rates for the
269 bioluminescent intensities in samples and standards were higher than that for the
270 negative control. The intensities measured for each respective standard were
271 determined after 5 h of incubation, and normalized against the intensities measured
272 from the negative control. This ratio was used to generate a calibration curve that
273 plotted the intensity ratio versus the concentration of (S)-4,5-dihydroxy-2,3-
274 pentanedione (DPD). The calibration curve was represented by the following
275 equation:
276 $y = 19.844 * x + 311.62$, with $R^2 = 0.994$
277 where y denotes intensity ratio, and x denotes the concentration of AI-2 in DPD
278 equivalence. Similarly, the intensities measured for each respective sample were
279 determined after 5 h of incubation and normalized against that from the negative
280 control. The ratio was then substituted into the equation to determine the AI-2
281 concentration present in that sample. AI-2 was measured in quadruplicates per
282 sample.

283 **2.7. DNA extraction and barcoded amplification of 16S rRNA genes**

284 The cell pellets obtained based on procedures described in Section 2.2 were
285 extracted for their genomic DNA using the UltraClean® Soil DNA Isolation Kit

286 (MoBio Laboratories,Carlsbad, USA) with slight modifications [32]. PCR
287 amplification for the 16S rRNA genes was performed with barcoded forward primer
288 515F (5′-GTGYCAGCMGCCGCGGTA-3′) and reverse primer 909R (5′-
289 CCCCGYCAATTCMTTTRAGT-3′) based on thermal cycling conditions
290 previously described [33]. All amplicons were of the correct size of ~450 bp and all
291 negative controls had no detectable amplification. Gel-purification of PCR amplicons
292 was performed with Wizard SV Gel and PCR Clean-up system (Promega, Madison,
293 USA). The amount of DNA in the purified amplicons was measured by Qubit® broad
294 range dsDNA assay (Invitrogen, Carlsbad, CA, USA). Equal amounts of the samples
295 were mixed together and submitted to Macrogen Korea for Ion Torrent sequencing
296 (Life Technologies, Carlsbad, USA) on 316 chips.

297 **2.8. Ion Torrent sequencing data analysis**

298 The sequencing data from Ion Torrent platforms were first sorted by the
299 KAUST Bioinformatics Team based on a Phred score of > 20. All primers, barcodes
300 and adapters as well as the sequences with < 350 nt were removed. Sequences that
301 passed the initial quality check were then evaluated for presence of chimeric
302 sequences using UCHIME [34]. The remaining chimera-free sequences were then
303 analyzed for their taxonomic affiliations at a 95% confidence level using the RDP
304 Classifier [35]. Chimera-free sequences were also collated with an in-house written
305 Perl script, and then sorted for unique operational taxonomic units (OTUs) at 97%
306 16S rRNA gene similarity using CD-Hit [36]. OTUs were blasted against the NCBI
307 16S rRNA gene nucleotide database using blastn to check for their closest matching
308 identities.

309 **2.9. Statistical analysis**

310 The extent of similarities between the microbial communities attached to the
311 aerobic and anaerobic MBR membranes were represented on a non-metric
312 multidimensional scaling (nMDS) plot. To generate the nMDS plot, the relative
313 abundances of the bacterial and archaeal genera were calculated, collated and then
314 square-root transformed. The square-root transformed dataset was then computed for
315 Bray-Curtis similarities and plotted on the nMDS. Vectors illustrated on the nMDS
316 exhibited a Pearson correlation of > 0.9 to the sample distribution. All measured
317 ATP, AI-2, protein and carbohydrate concentration data were also collated, log-
318 transformed and normalized prior to principal component analysis (PCA). The four
319 measured parameters (i.e., ATP, AI-2, protein and carbohydrate) were displayed as
320 vectors on the PCA to illustrate the contribution of each parameter in the distribution
321 of samples on the plot. All statistical analysis described in this section was performed
322 on Primer-E v7 software [37].

323 **2.10. Nucleotide sequence accession numbers**

324 All high-throughput sequencing files were deposited in the Short Read Archive
325 (SRA) of the European Nucleotide Archive (ENA) under study accession number
326 PRJEB9458.

327

3. Results

3.1. AeMBR and AnMBR operational performances

The AeMBR and AnMBR systems achieved an average COD removal efficiency of 94% and 90%, respectively (Figure S1). The TMP in the AeMBR system increased to 52 kPa at the end of 3 weeks of continuous operation (Figure 2), while the TMP measured for the membranes connected to the AeMBR at the end of 4 weeks and 5 weeks was 88 kPa for both. For the AnMBR system, the TMP gradually increased from 0 kPa to 23 kPa and 62 kPa at the end of 3, 6 and 9 weeks, respectively (Figure 2). Membranes were harvested from the AeMBR at time intervals of 3 weeks, 4 weeks and 5 weeks, and at time intervals of 3 weeks, 6 weeks and 9 weeks for the AnMBR to represent comparable levels of fouling for both systems.

3.2. Protein and carbohydrate concentration in retentate and permeate streams of AeMBR and AnMBR

The amount of total protein and carbohydrate in retentate from the AeMBR was on average 7.2 ± 1.3 mg/L and 21.8 ± 2.7 mg/L, respectively, throughout operation (Figure 3A). The amount of protein and carbohydrate in AeMBR retentate was lower than that detected in the AnMBR retentate. The average amount of protein in AnMBR retentate was 94.1 ± 24.7 mg/L while the amount of carbohydrate in the AnMBR retentate exhibited a gradual increase from 22.6 ± 2.9 mg/L during days 0 to 40 of operation to 51.2 ± 7.5 mg/L from day 40 onwards (Figure 3B). The amount of total carbohydrate in AeMBR permeate was 76.5% of that detected in the retentate, and was significantly lower in the permeate (t-test, $P < 0.05$). However, the amount of

protein in permeate and retentate of the AeMBR was not significantly different (t-test, $P = 0.65$). In contrast, up to 89.2% of protein and 91.3% of carbohydrate were removed from the AnMBR retentate, and a significant reduction for both protein and carbohydrate was observed in the AnMBR permeate compared to retentate (t-test, $P < 0.05$).

3.3. Protein and carbohydrate concentration in soluble EPS of attached biomass

The amount of carbohydrate measured in soluble EPS extracted from different portions of the 3-week aerobic membranes ranged from 70-102 mg/L. There was a comparatively higher concentration of carbohydrate than protein in the soluble EPS of aerobic membranes. Furthermore, the amount of carbohydrate increased to 102-126 mg/L and 173-197 mg/L in the 4-week and 5-week aerobic membranes, respectively (Figure 3C). These carbohydrate concentrations detected in both 4-week and 5-week membranes were significantly higher than that detected in 3-week membranes (t-test, $P < 0.05$). The average protein content in 3-week and 4-week aerobic membranes was 40.5 ± 5.2 and 36.1 ± 6.0 mg/L, respectively, and significantly increased (t-test, $P < 0.05$) to 67-74 mg/L in the 5-week aerobic membranes (Figure 3C). In contrast, more protein than carbohydrate was present in the soluble EPS of anaerobic membranes (Figure 3D). There was a significant increase in both carbohydrate and protein concentrations detected in the soluble EPS of 6-week and 9-week anaerobic membranes compared to the 3-week membrane (t-test, $P <0.05$). A slight increase of carbohydrate was also observed between the 6-week and 9-week anaerobic membranes (t-test, $P = 0.09$) but no significant difference was observed for protein (t-test, $P = 0.46$).

3.4. Molecular Weight (MW)-based fingerprinting profiles of SMP and soluble EPS in AeMBR

A single-peak fragment of 0.9 kDa was detected in the retentate and permeate throughout the course of AeMBR operation (Figure 4A). The peak area for this fragment was similar for both AeMBR retentate and permeate, indicating that this fragment had completely permeated through the PVDF MF membrane. Unlike the MW-based fingerprinting profile of AeMBR SMP, the protein components present in the soluble EPS of aerobic membranes had a bimodal distribution of the MW fragments (Figure 4C). A single-peak fragment of 487.8 ± 43.9 kDa was observed in the 3 and 4 weeks membranes, in contrast to two peaks on the 5 weeks aerobic membrane that were comprised of the original fragment and an additional 837.7 kDa fragment. In addition, fragments of small MW ranging from 0.01-4 kDa were observed on all aerobic MBRs but were not detected in the SMP of AeMBR (Figure 4C). The carbohydrates detected in both SMP and soluble EPS of AeMBR shared different fingerprinting profiles (Figure 4B and 4D). A single peak associated with an average MW of 180.1 ± 5.5 kDa was also observed in the SMP (Figure 4B) but not in the soluble EPS fraction (Figure 4D). Instead, two main fragments of MW 3396.6 ± 64.4 kDa kDa and 94.9 ± 9.7 kDa were the main polysaccharide compounds detected on the soluble EPS of aerobic membranes.

3.5. Molecular weight (MW)-based fingerprinting profiles of SMP and soluble EPS in AnMBR

SMP and soluble EPS of the AnMBR exhibited different fingerprinting profiles compared to those of the AeMBR (Figure 5). The pattern of MW fingerprints

397 of protein in SMP in the AnMBR was similar to those in EPS of anaerobic
398 membranes (Figure 5A and 5C). Both had a single peak and a bigger MW size
399 ranging from 630-640 kD. This fragment in SMP was completely rejected by the MF
400 membrane. Given that this specific fragment was ubiquitously detected in the
401 AnMBR system, the fragment was further extracted for peptide sequencing. Out of
402 the 80 total peptide sequences obtained, 57.5% of the sequences were identified to be
403 vitellogenin, which is a glycoliproprotein (Supplementary Material).

404 Among the three detected polysaccharide fractions in the SMP of AnMBR,
405 only the first eluted fragment with the biggest MW (average 2526.3 ± 483.4 kDa) was
406 completely rejected by the MF membrane (Figure 5B). However, even though the
407 2526.3 kDa polysaccharide fragment was rejected by the anaerobic membranes, this
408 fragment was not detected in the soluble EPS of the membranes (Figure 5D). The
409 majority of the fragment with a MW size of 0.17 kDa was retained in the reactor. The
410 fragment with a size of 158.5 ± 6.5 kDa was low in abundance in the SMP but
411 increased in abundance within the soluble EPS of the anaerobic membranes with time,
412 and constituted one of the two peaks detected (Figure 5D).

413 **3.6. ATP and AI-2 in AeMBR and AnMBR**

414 The amount of ATP measured in the biocake layer on aerobic membranes was
415 at least 3-fold higher than that measured on anaerobic membranes (Figure 6A and
416 6B). The ATP content for all three sessions in AnMBR membranes was less than 100
417 pmol/cm^2, while 300 to 1500 pmol/cm^2 ATP was measured in the biocake on the 3-
418 week to 5-week AeMBR membranes. The amount of ATP on the aerobic membranes
419 increased with time but there was no significant difference between the amount of

ATP on the 5-week aerobic membrane compared to 3-week aerobic membrane (t-test, P = 0.07). There was also no significant change of AI-2 content among the different aerobic membranes (t-test, P > 0.25). The average AI-2 in the biocake of all aerobic membranes was 0.2 nmol/cm^2, while a temporal increase in AI-2 content was observed for the anaerobic membranes. The AI-2 concentration in the 3-week anaerobic membrane was less than 0.2 nmol/cm^2 while the average amount of AI-2 in the 6-week anaerobic membrane was 0.4 nmol/cm^2. The average amount of AI-2 further increased in the 9-week anaerobic membrane to 0.83 nmol/cm^2, and was significantly higher than that detected from the 3-week anaerobic membrane (t-test, P = 0.03).

3.7. Microbial community on AeMBR and AnMBR membranes

The aerobic and anaerobic membranes were evaluated for their extent of dissimilarities based on the measured concentrations of ATP, AI-2, carbohydrate and protein in the biocake (Figure 7A), as well as relative abundance and occurrence of bacterial populations attached to the membranes (Figure 7B), Based on both evaluation approaches, it was observed that the biocake properties and the microbial communities of the aerobic membranes were distinctly different from those of the anaerobic membranes. To illustrate, aerobic and anaerobic samples were spatially clustered apart on the PCA plot along the PC1 axis, which accounted for 54.9% of the total variance. The main vectors that accounted for the spatial distribution of the aerobic samples on the PCA were the concentrations of ATP and carbohydrate. In particular, the amount of ATP and carbohydrate in the biocake of aerobic membranes was higher than that detected in the anaerobic membranes. A similar distribution of

443 the microbial communities attached to aerobic and anaerobic membranes was
444 observed on the MDS plot. Unclassified Syntrophaceae was one of the two bacterial
445 populations that was highly correlated ($\rho = 0.9$) with the positioning of 9-week
446 anaerobic samples on the nMDS. Further evaluation showed that an OTU with a best-
447 matched identity to *Smithella propionica* (i.e., a syntroph) increased in its relative
448 abundance from 0.27% on a 3-week anaerobic membrane to 1.2% on a 9-week
449 anaerobic membrane. In contrast, the abundance of unclassified Comamonadaceae
450 (e.g. *Comamonas testosteroni*) and unclassified Chitinophagaceae (e.g.
451 *Ferruginibacter lapsinanis*, *Terrimonas rubra*) highly correlated with the spatial
452 distribution of the aerobic membranes. Collectively, these three OTUs accounted for
453 up to 13.6% of the total microbial community attached to the most fouled 5-week
454 aerobic membrane (Table 1). The concentration of ATP in the biocake was further
455 identified as the single variable that best linked the spatial distribution of samples on
456 the PCA plot with those on the MDS plot (correlation value = 0.698, $p = 0.001$).

457 **4. Discussion**

458 In recent years, there has been increasing interest in AnMBRs due to the
459 various advantages associated with the coupling of membrane separation to anaerobic
460 fermentation processes. As is the case with all membrane bioreactors, membrane
461 fouling remains a significant obstacle limiting their widespread use. It has
462 conventionally being presumed that the fouling mechanisms between aerobic and
463 anaerobic systems are similar, at least at the macro scale [21]. Unlike past studies,
464 which examined fouling rates in CSTR-type AeMBRs, this study evaluated the
465 differences in the fouling rates of AeMBR and AnMBR operated based on an

466 attached-growth reactor configuration. This is built upon past observations which
467 reported a lower MLSS resulting from attached-growth reactors playing a positive
468 role in controlling membrane fouling in AeMBR systems [22]. However, our results
469 showed that when an AeMBR was evaluated against an AnMBR system with the
470 same reactor configuration, the fouling rates and mechanisms experienced by their
471 respective membranes were very different, despite both systems achieving similar
472 COD removal efficiencies.

473 Compared to the AeMBR, more gradual membrane fouling was observed in
474 the AnMBR. TMP in the AeMBR increased to over 90 kPa after 4 weeks of
475 operation, while TMP in the AnMBR did not reach similar levels until after 9 weeks
476 of operation (Figure 2). Correlating with the TMP increment, aerobic membranes
477 were more severely fouled after 4 and 5 weeks of operation as compared to the 3-
478 week membrane, with significantly higher protein and carbohydrate contents in the 4-
479 week and 5-week aerobic membranes than the 3-week membrane. Similarly, the 6-
480 week and 9-week anaerobic membranes exhibited significantly higher protein and
481 carbohydrate contents than that of the membrane removed after 3 weeks of operation
482 (Figure 3).

483 The slower fouling rates in the AnMBR system may be due to a lower solids
484 deposition rate on the anaerobic membrane surface than the aerobic membrane [5].
485 This was in spite of the overall SMP levels in the AnMBR being almost 5 times
486 higher than in the AeMBR reactor (Figure 3), and that a high abundance of SMP had
487 been shown previously to correlate to membrane fouling [38]. A previous study
488 comparing AeMBR and AnMBR systems reported SMP levels that were up to 6

489 times higher in the AnMBR, and that the AnMBR experienced more rapid membrane
490 fouling [39]. However, our findings did not show any correlation between the
491 abundance of SMP and extent of membrane fouling. This implies that, although SMP
492 is known to contribute significantly to membrane fouling rates, absolute
493 quantification of SMP may not be as important as its specific components.
494 Conversely, soluble EPS (i.e., SMP associated with the attached biomass) examined
495 in this study had levels that correlated positively with the membrane fouling rates,
496 both in terms of raw quantification (Figure 3) and specific protein and polysaccharide
497 fractionation profiles (Figure 4 and 5).

498 Based on fractionation profiles, it was observed that the AnMBR produced
499 bigger molecular weight fractions in its SMP than the aerobic process. This, in turn,
500 resulted in the majority of the proteins and carbohydrates being retained in the
501 anaerobic retentate. Protein subsequently accumulated on the fouled anaerobic
502 membranes, and was comprised of a single fraction with a MW size of 633 kDa
503 (Figure 5C). This protein fragment was further determined from peptide sequencing
504 to be made up by glycolipoprotein (Supplementary Material). It is to be noted that
505 although the MW 633 kDa was less than the physical pore size of 0.3μm of PVDF
506 membrane, HPLC analysis indicated that this fragment was totally rejected by the
507 AnMBR membrane. A similar occurrence was also observed in a study by Jang et al.,
508 where it was found that a MF membrane with pore size of 0.4 μm could retain
509 biopolymers of MW as low as 40 kDa [40]. Electrostatic repulsion may be a factor in
510 causing the rejection of biopolymers of sizes smaller than the physical pore size of
511 membranes [41]. Another contributing factor could be related to the deposited

biofoulants on the membrane surface, as seen in studies where the biofilm layer acted as a secondary self-forming dynamic membrane that modified the membrane's rejection properties [42-45].

This phenomenon would also likely explain the partial rejection of a polysaccharide compound of 0.17 kDa MW that was also found in the AnMBR-SMP, implying that in certain instances properties such as particle charge, hydrophobicity, and aggregation completely supersede physical rejection by the porous membrane. Although the 0.17 kDa compound was rejected by the anaerobic membrane, an associated fragment of the same size was not observed within the soluble EPS of the anaerobic membrane (Figure 5). Instead, the 158 kDa polysaccharide fragment, which was observed in low abundances in the SMP, built up within the soluble EPS associated with the attached biomass on anaerobic membranes. In addition, a polysaccharide component of 4308 kDa MW increased in abundance as the anaerobic membrane became increasingly fouled with time. This compound was not observed in the SMP and could not be easily traced. It is possible that this large size MW fragment may be comprised of a complex of inorganic and organic foulants that combined to form a fragment of this size. Past studies have shown that anaerobic MBRs are more prone to inorganic fouling due to the high ammonium and phosphate content within the reactor [46]. Inorganic foulants such as struvite, otherwise also known as magnesium ammonium phosphate hexahydrate ($MgNH_4PO_4 \cdot 6H_2O$), were thought to contribute to polysaccharide accumulation due to the free positive ions binding to the negative charges of OH^- and COO^- that may be present among extracellular polysaccharide molecules [47].

Unlike the anaerobic membrane, the aerobic membrane displayed SMP MW profiles that were very different from those of the soluble EPS of the fouled membranes in terms of both proteins and carbohydrates. To illustrate, there were no apparent soluble EPS fragments that could be traced to SMP counterparts in the AeMBR reactor (Figure 4). The sole protein and polysaccharide fragments detected in the SMP were completely permeated through the membrane in the AeMBR, suggesting that the aerobic sludge produced SMP fragments with physical properties that reduced interactions with the MF membranes used.

Results of ATP quantification of the biofilms further suggest that the mechanism for biofouling in the AeMBR system could be completely different from that of the AnMBR system. Instead of SMP compound deposition on the membrane like what had been observed for the anaerobic membrane, it appeared that activity of the localized microbial communities and their EPS production could be responsible for the majority of the soluble EPS on the AeMBR membrane surface. To illustrate, ATP levels per surface area in the AeMBR were significantly higher (> 30 fold) than those in the AnMBR (Figure 6A). This relatively higher ATP content in the AeMBR membrane biofilms demonstrates that microbial activity is also likely much higher [48, 49]. A large fraction of the EPS on the AeMBR membranes could be attributed to this microbial activity as higher biomass activity is generally associated with higher specific soluble EPS production rates [50]. Considering these observations, in combination with the previously discussed protein and polysaccharide fragment analyses that showed little similarity between the soluble EPS and SMP profiles for

557 the AeMBR, it seems likely that the main contributors to membrane fouling in the
558 AeMBR arise from microbial activity on the membranes.
559 An evaluation of the microbial communities showed that the abundance of
560 unclassified Comamonadaceae (e.g. *Comamonas testosteroni*) and unclassified
561 Chitinophagaceae (e.g. *Ferruginibacter lapsinanis*, *Terrimonas rubra*) were the main
562 bacterial vectors that resulted in the separation of the aerobic membrane samples from
563 those of the anaerobic membranes in MDS analysis (Figure 7B). Collectively, the
564 three OTUs most likely representing these bacterial groups accounted for up to 13.6%
565 of the total microbial community attached to the most seriously fouled 5-week
566 aerobic membrane (Table 1), suggesting that they may play a role in the aerobic
567 membrane fouling process. Past studies have reported the presence of *Comamonas*
568 spp. in the biofilms of aerobic membranes [51]. Furthermore, a significantly higher
569 abundance of *Comamona*s spp. and *Ferruginibacter* spp. have been observed in
570 aerobic sludge samples taken from an MBR fed with influent wastewater of a higher
571 COD/N ratio than ones taken from an MBR fed with a lower COD/N ratio [20].
572 These observations suggest that these two bacterial populations could preferentially
573 attach to aerobic membrane surfaces, where dense organic matter is likely to
574 accumulate. In a related study, clone library analysis similarly revealed that
575 Betaproteobacteria (*Comamona*s) and Bacteroidetes (*Ferruginibacter*) were the
576 dominant groups in aerobic MBR membrane biofilms [52]. Given the positive
577 correlation between ATP concentrations and the abundance of *Comamonas* spp. and
578 Chitinophagaeceae ($\rho = 0.698$, $p = 0.001$), it is likely that these two bacterial

579 populations were contributing to the bioactivity on the aerobic membrane surfaces,
580 resulting in an increase in ATP levels.

581 This study did not look into the insoluble portions of membrane biofilm EPS,
582 which generally account for a relatively larger portion of the EPS matrix than the
583 soluble fractions. Neither did the study comprehensively characterize the bound EPS
584 from the biofilm cake layers and suspended mixed liquor in the fouling of both MBR
585 types. Furthermore, it is likely that the extraction method used in this study did not
586 recover all of the protein and polysaccharide components present in the SMP and
587 soluble EPS. In a study by Aquino and Stuckey that used liquid-liquid extraction
588 protocols with various organic solvents, up to 20 MW fragments ranging from 10 kDa
589 to over 300 kDa in the soluble microbial products of AnMBR effluent were identified
590 [53]. Further studies on the insoluble EPS and tightly-bound EPS extracted from
591 different protocols may develop new and improved insight on the different membrane
592 fouling mechanisms. Despite these limitations, this study revealed significant
593 differences between aerobic and anaerobic MBRs in the fractions of SMP and soluble
594 EPS measured that shed light on the mechanisms potentially responsible for fouling.

595 Given the observed differences in the fouling mechanisms of both systems,
596 different membrane fouling control approaches can be recommended accordingly.
597 Since the mechanisms most responsible for membrane fouling in AnMBRs are SMP
598 deposition, as shown in this study, and cake formation [54], conventional chemical or
599 physical cleaning methods could be effective AnMBR fouling control techniques. For
600 example, addition of $FeCl_3$ reduced the accumulation of protein and carbohydrate on
601 AnMBR membrane surfaces, leading to lower fouling rates. It was proposed that

602 $FeCl_3$ acts as a coagulant for colloidal and soluble substances, and prevented the
603 development of a strongly-attached cake layer on the anaerobic membranes [55].
604 Recent studies have also utilized granular activated carbon (GAC) to reduce AnMBR
605 membrane fouling by providing mechanical scouring to the membrane surfaces [56-
606 58] and have demonstrated that the AnMBR can be operated continuously for up to 6
607 months at 6-11 LMH with no significant increases in TMP [57]. Similarly,
608 mechanical air scouring methods have been used extensively for mitigation of
609 membrane fouling in aerobic MBRs [59, 60]. To compliment these methods,
610 biological-based approaches can be used to further prolong membrane life in
611 AeMBRs. Examples of such approaches include quenching of acyl-homoserine
612 lactone (AHL) and AI-2 signal molecules to inhibit cell-to-cell communication within
613 the biofilm matrix and addition of enzymes to break down proteins and
614 polysaccharides of the biofilm [61-65]. One study showed that by encapsulating
615 *Rhodococcus* sp. or recombinant *E. coli* in microbial vessels as a live source of
616 quorum quenching inside the MBR, the emitted quorum quenchers were able to delay
617 the occurrence of maximum TMP by up to a day as compared to the control AeMBR
618 [61, 64].

619 **5. Conclusion**

620 Although high COD removal efficiency was achieved for both aerobic and
621 anaerobic MBR systems, faster membrane fouling was observed in the AeMBR. The
622 MW fingerprints of SMP and EPS in the AnMBR showed that a majority of EPS
623 fragments could be derived from the retained SMP fractions, implying that the major
624 contributor to AnMBR membrane fouling was physical retention of SMP components

by the microfiltration membrane. In the case of the AeMBR, all SMP fragments were completely permeated through the membrane and EPS did not correlate with SMP profiles. Furthermore, significantly higher levels of ATP were present in AeMBR membrane biofilms than in those of the AnMBR, suggesting that a larger fraction of the EPS on the AeMBR membrane was a product of microbial activity arising from certain bacterial populations on the membrane surfaces, such as *Comamonas* and unclassified Chitinophagaceae. This study shows that potentially very different fouling mechanisms controlled AeMBR and AnMBR membrane biofouling and reiterates the importance of a multifaceted approach in studying membrane fouling and developing control strategies for different MBR systems.

6. Acknowledgements

The authors would like to thank KAUST Proteomics core lab for their technical assistance. This study was funded by the KAUST Center Competitive Funding Program grant (FCC/1/1971-06-01) awarded to P-Y Hong.

References

[1] H.Y. Ng, T.W. Tan, S.L. Ong, Membrane fouling of submerged membrane bioreactors: impact of mean cell residence time and the contributing factors, Environmental science & technology, 40 (2006) 2706-2713.

[2] E.B. Muller, A.H. Stouthamer, H.W. Vanverseveld, D.H. Eikelboom, Aerobic Domestic Waste-Water Treatment in a Pilot-Plant with Complete Sludge Retention by Cross-Flow Filtration, Water Res, 29 (1995) 1179-1189.

[3] S. Judd, Introduction, in: The MBR Book: Principles and Applications of Membrane Bioreactors for Water and Wastewater Treatment, Elsevier Science, 2010, pp. 1-55.

[4] B.-Q. Liao, J.T. Kraemer, D.M. Bagley, Anaerobic Membrane Bioreactors: Applications and Research Directions, Critical Reviews in Environmental Science and Technology, 36 (2006) 489-530.

[5] S.H. Baek, K.R. Pagilla, Aerobic and anaerobic membrane bioreactors for municipal wastewater treatment, Water environment research, (2006) 133-140.

[6] B.D. Shoener, I.M. Bradley, R.D. Cusick, J.S. Guest, Energy positive domestic wastewater treatment: the roles of anaerobic and phototrophic technologies, Environmental science. Processes & impacts, 16 (2014) 1204-1222.

[7] A.L. Smith, L.B. Stadler, N.G. Love, S.J. Skerlos, L. Raskin, Perspectives on anaerobic membrane bioreactor treatment of domestic wastewater: a critical review, Bioresource technology, 122 (2012) 149-159.

[8] T.-H. Bae, T.-M. Tak, Interpretation of fouling characteristics of ultrafiltration membranes during the filtration of membrane bioreactor mixed liquor, J Membrane Sci, 264 (2005) 151-160.

[9] L. Defrance, M.Y. Jaffrin, B. Gupta, P. Paullier, V. Geaugey, Contribution of various constituents of activated sludge to membrane bioreactor fouling, Bioresource technology, 73 (2000) 105-112.

[10] E. Namkung, B.E. Rittmann, Soluble Microbial Products (Smp) Formation Kinetics by Biofilms, Water Res, 20 (1986) 795-806.

[11] H.C. Flemming, J. Wingender, Relevance of microbial extracellular polymeric substances (EPSs)--Part I: Structural and ecological aspects, Water science and technology : a journal of the International Association on Water Pollution Research, 43 (2001) 1-8.

[12] C.S. Laspidou, B.E. Rittmann, A unified theory for extracellular polymeric substances, soluble microbial products, and active and inert biomass, Water Res, 36 (2002) 2711-2720.

[13] D. Bhatia, I. Bourven, S. Simon, F. Bordas, E.D. van Hullebusch, S. Rossano, P.N. Lens, G. Guibaud, Fluorescence detection to determine proteins and humic-like substances fingerprints of exopolymeric substances (EPS) from biological sludges performed by size exclusion chromatography (SEC), Bioresource technology, 131 (2013) 159-165.

[14] N. Cicek, M.T. Suidan, P. Ginestet, J.M. Audic, Impact of soluble organic compounds on permeate flux in an aerobic membrane bioreactor, Environmental technology, 24 (2003) 249-256.

[15] S. Rosenberger, C. Laabs, B. Lesjean, R. Gnirss, G. Amy, M. Jekel, J.C. Schrotter, Impact of colloidal and soluble organic material on membrane performance in membrane bioreactors for municipal wastewater treatment, Water Res, 40 (2006) 710-720.

[16] A. Drews, M. Vocks, V. Iversen, B. Lesjean, M. Kraume, Influence of unsteady membrane bioreactor operation on EPS formation and filtration resistance, Desalination, 192 (2006) 1-9.

[17] S. Arabi, G. Nakhla, Impact of protein/carbohydrate ratio in the feed wastewater on the membrane fouling in membrane bioreactors, J Membrane Sci, 324 (2008) 142-150.

[18] E. Bouhabila, R. Ben Aim, H. Buisson, Fouling characterisation in membrane bioreactors, Sep Purif Technol, 22-3 (2001) 123-132.

[19] S. Rosenberger, H. Evenblij, S.T. Poele, T. Wintgens, C. Laabs, The importance of liquid phase analyses to understand fouling in membrane assisted activated sludge processes - six case studies of different European research groups, J Membrane Sci, 263 (2005) 113-126.

[20] X. Han, Z. Wang, J. Ma, C. Zhu, Y. Li, Z. Wu, Membrane bioreactors fed with different COD/N ratio wastewater: impacts on microbial community, microbial products, and membrane fouling, Environmental science and pollution research international, (2015).

[21] D.C. Stuckey, Recent developments in anaerobic membrane reactors, Bioresource technology, 122 (2012) 137-148.

[22] A. Achilli, E.A. Marchand, A.E. Childress, A performance evaluation of three membrane bioreactor systems: aerobic, anaerobic, and attached-growth, Water Science and Technology, 63 (2011) 2999-3005.

[23] C.-H. Wei, M. Harb, G. Amy, P.-Y. Hong, T. Leiknes, Sustainable organic loading rate and energy recovery potential of mesophilic anaerobic membrane bioreactor for municipal wastewater treatment, Bioresource technology, 166 (2014) 326-334.

[24] I. Nopens, C. Capalozza, P.A. Vanrolleghem, Stability analysis of a synthetic municipal wastewater, Department of Applied Mathematics Biometrics and Process Control, University of Gent, Belgium, (2001).

[25] M. Dubios, K.A. Gilles, J.K. Hamilton, P.A. Rebers, F. Smith, Colorimetric method for determination of sugar and related substances, Analytical Chemistry, 28 (1956) 350-356.

[26] T. Görner, P. de Donato, M.-H. Ameil, E. Montarges-Pelletier, B.S. Lartiges, Activated sludge exopolymers: separation and identification using size exclusion chromatography and infrared micro-spectroscopy, Water Res, 37 (2003) 2388-2393.

[27] R. Mempin, H. Tran, C. Chen, H. Gong, K.K. Ho, S. Lu, Release of extracellular ATP by bacteria during growth, BMC microbiology, 13 (2013) 301.

[28] J.-G. Cao, E. Meighen, Purification and structural identification of an autoinducer for the luminescence system of Vibrio harveyi, Journal of Biological Chemistry, 264 (1989) 21670-21676.

[29] A.F.G. Barrios, R. Zuo, Y. Hashimoto, L. Yang, W.E. Bentley, T.K. Wood, Autoinducer 2 controls biofilm formation in Escherichia coli through a novel motility quorum-sensing regulator (MqsR, B3022), Journal of bacteriology, 188 (2006) 305-316.

[30] N. Ahmed, F. Petersen, A.A. Scheie, Biofilm formation and autoinducer‐2 signaling in Streptococcus intermedius: role of thermal and pH factors, Oral microbiology and immunology, 23 (2008) 492-497.

[31] Y. Xiong, Y. Liu, Involvement of ATP and autoinducer‐2 in aerobic granulation, Biotechnology and bioengineering, 105 (2010) 51-58.

[32] P.-Y. Hong, E. Wheeler, I.K. Cann, R.I. Mackie, Phylogenetic analysis of the fecal microbial community in herbivorous land and marine iguanas of the Galápagos Islands using 16S rRNA-based pyrosequencing, The ISME journal, 5 (2011) 1461-1470.

[33] N. Al-Jassim, M.I. Ansari, M. Harb, P.-Y. Hong, Removal of bacterial contaminants and antibiotic resistance genes by conventional wastewater treatment processes in Saudi Arabia: Is the treated wastewater safe to reuse for agricultural irrigation?, Water research, 73 (2015) 277-290.

[34] R.C. Edgar, B.J. Haas, J.C. Clemente, C. Quince, R. Knight, UCHIME improves sensitivity and speed of chimera detection, Bioinformatics, 27 (2011) 2194-2200.

[35] Q. Wang, G.M. Garrity, J.M. Tiedje, J.R. Cole, Naive Bayesian classifier for rapid assignment of rRNA sequences into the new bacterial taxonomy, Applied and environmental microbiology, 73 (2007) 5261-5267.

[36] W. Li, A. Godzik, Cd-hit: a fast program for clustering and comparing large sets of protein or nucleotide sequences, Bioinformatics, 22 (2006) 1658-1659.

[37] K. Clarke, R. Gorley, PRIMER version 7: user manual/tutorial, PRIMER-E, Plymouth, UK, 192 (2015) 296.

[38] R.S. Trussell, R.P. Merlo, S.W. Hermanowicz, D. Jenkins, The effect of organic loading on process performance and membrane fouling in a submerged membrane bioreactor treating municipal wastewater, Water Research, 40 (2006) 2675-2683.

[39] I. Martin-Garcia, V. Monsalvo, M. Pidou, P. Le-Clech, S. Judd, E. McAdam, B. Jefferson, Impact of membrane configuration on fouling in anaerobic membrane bioreactors, J Membrane Sci, 382 (2011) 41-49.

[40] N. Jang, H. Shon, X. Ren, S. Vigneswaran, I.S. Kim, Characteristics of Soluble Foulants in the Membrane Bioreactor (MBR), (2006).

[41] S. Allgeier, B. Alspach, J. Vickers, Membrane filtration guidance manual, United States Environmental Protection Agency, US, (2005).

[42] H. Harada, K. Momonoi, S. Yamazaki, S. Takizawa, Application of anaerobic-UF membrane reactor for treatment of a wastewater containing high strength particulate organics, Water Science and Technology, 30 (1994) 307-319.

[43] V. Pillay, B. Townsend, C. Buckley, Improving the performance of anaerobic digesters at wastewater treatment works: The coupled cross-flow microfiltration/digester process, Water science and technology, 30 (1994) 329-337.

[44] H. Choi, K. Zhang, D.D. Dionysiou, D.B. Oerther, G.A. Sorial, Influence of cross-flow velocity on membrane performance during filtration of biological suspension, J Membrane Sci, 248 (2005) 189-199.

[45] D. Jeison, I. Díaz, J.B. van Lier, Anaerobic membrane bioreactors: Are membranes really necessary?, Electronic Journal of Biotechnology, 11 (2008) 1-2.

[46] H. Lin, W. Peng, M. Zhang, J. Chen, H. Hong, Y. Zhang, A review on anaerobic membrane bioreactors: applications, membrane fouling and future perspectives, Desalination, 314 (2013) 169-188.

[47] G.W. Wang, D. Wang, X.C. Xu, F.L. Yang, Partial nitrifying granule stimulated by struvite carrier in treating pharmaceutical wastewater, Appl Microbiol Biot, 97 (2013) 8757-8765.

[48] J.-I. Horiuchi, K. Ebie, K. Tada, M. Kobayashi, T. Kanno, Simplified method for estimation of microbial activity in compost by ATP analysis, Bioresource technology, 86 (2003) 95-98.

[49] K. Ochromowicz, E.J. Hoekstra, ATP as an indicator of microbiological activity in tap water, European Commision Directorate–General Joint Research Centre, (2005).

[50] H. Xu, K. Teo, H. Neo, Y. Liu, Chemically inhibited ATP synthesis promoted detachment of different-age biofilms from membrane surface, Applied microbiology and biotechnology, 95 (2012) 1073-1082.

[51] M.C. Gao, M. Yang, H.Y. Li, Q.X. Yang, Y. Zhang, Comparison between a submerged membrane bioreactor and a conventional activated sludge system on treating ammonia-bearing inorganic wastewater, J Biotechnol, 108 (2004) 265-269.

[52] S. Xia, J. Li, S. He, K. Xie, X. Wang, Y. Zhang, L. Duan, Z. Zhang, The effect of organic loading on bacterial community composition of membrane biofilms in a submerged polyvinyl chloride membrane bioreactor, Bioresource technology, 101 (2010) 6601-6609.

[53] S.F. Aquino, D.C. Stuckey, Characterization of soluble microbial products (SMP) in effluents from anaerobic reactors, Water science and technology : a journal of the International Association on Water Pollution Research, 45 (2002) 127-132.

[54] A. Charfi, N. Ben Amar, J. Harmand, Analysis of fouling mechanisms in anaerobic membrane bioreactors, Water Res, 46 (2012) 2637-2650.

[55] Q. Dong, W. Parker, M. Dagnew, Impact of FeCl 3 dosing on AnMBR treatment of municipal wastewater, Water Research, 80 (2015) 281-293.

[56] M.A. Johir, S. Shanmuganathan, S. Vigneswaran, J. Kandasamy, Performance of submerged membrane bioreactor (SMBR) with and without the addition of the different particle sizes of GAC as suspended medium, Bioresource technology, 141 (2013) 13-18.

[57] R. Yoo, J. Kim, P.L. McCarty, J. Bae, Anaerobic treatment of municipal wastewater with a staged anaerobic fluidized membrane bioreactor (SAF-MBR) system, Bioresource technology, 120 (2012) 133-139.

[58] J. Kim, K. Kim, H. Ye, E. Lee, C. Shin, P.L. McCarty, J. Bae, Anaerobic fluidized bed membrane bioreactor for wastewater treatment, Environmental science & technology, 45 (2011) 576-581.

[59] J.-P. Nywening, H. Zhou, Influence of filtration conditions on membrane fouling and scouring aeration effectiveness in submerged membrane bioreactors to treat municipal wastewater, Water research, 43 (2009) 3548-3558.

[60] L. Böhm, A. Drews, H. Prieske, P.R. Bérubé, M. Kraume, The importance of fluid dynamics for MBR fouling mitigation, Bioresource technology, 122 (2012) 50-61.

[61] K.M. Yeon, C.H. Lee, J. Kim, Magnetic enzyme carrier for effective biofouling control in the membrane bioreactor based on enzymatic quorum quenching, Environmental science & technology, 43 (2009) 7403-7409.

[62] K.M. Yeon, W.S. Cheong, H.S. Oh, W.N. Lee, B.K. Hwang, C.H. Lee, H. Beyenal, Z. Lewandowski, Quorum sensing: a new biofouling control paradigm in a membrane bioreactor for advanced wastewater treatment, Environmental science & technology, 43 (2009) 380-385.

[63] H.S. Oh, K.M. Yeon, C.S. Yang, S.R. Kim, C.H. Lee, S.Y. Park, J.Y. Han, J.K. Lee, Control of membrane biofouling in MBR for wastewater treatment by quorum quenching bacteria encapsulated in microporous membrane, Environmental science & technology, 46 (2012) 4877-4884.

[64] D. Jahangir, H.S. Oh, S.R. Kim, P.K. Park, C.H. Lee, J.K. Lee, Specific location of encapsulated quorum quenching bacteria for biofouling control in an external submerged membrane bioreactor, J Membrane Sci, 411 (2012) 130-136.

[65] W. Jiang, S.Q. Xia, J. Liang, Z.Q. Zhang, S.W. Hermanowicz, Effect of quorum quenching on the reactor performance, biofouling and biomass characteristics in membrane bioreactors, Water Res, 47 (2013) 187-196.

Figure captions

Figure 1. Operational setup for both aerobic MBR and anaerobic MBR. An attached-growth reactor configuration was used and the MBR systems were operated at 18.5 h hydraulic retention time (HRT) and with flux of 6-8 $L/m^2/h$ through the microfiltration (MF) membrane.

Figure 2. Transmembrane pressure (TMP) measured throughout the operation of AeMBR and AnMBR. Aerobic membranes were harvested after 3, 4 and 5 weeks of operation at different final TMP. Anaerobic membranes were harvested after 3, 6 and 9 weeks of operation at different final TMP.

Figure 3. The concentration of proteins, PN, and carbohydrates, CH, in **(A)** retentate and permeate of aerobic MBR, AeMBR **(B)** retentate and permeate of anaerobic MBR, AnMBR **(C)** soluble EPS from different sections of aerobic membranes **(D)** soluble EPS from different sections of anaerobic membranes.

Figure 4. Molecular weight fingerprinting profiles of **(A)** proteins in SMP of aerobic MBR retentate and permeate, **(B)** carbohydrates in SMP of aerobic MBR retentate and permeate **(C)** proteins in soluble EPS of aerobic membranes, and **(D)** carbohydrates in soluble EPS of aerobic membranes.

Figure 5. Molecular weight fingerprinting profiles of **(A)** proteins in SMP of anaerobic MBR retentate and permeate, **(B)** carbohydrates in SMP of anaerobic MBR retentate and permeate **(C)** proteins in soluble EPS of anaerobic membranes, and **(D)** carbohydrates in soluble EPS of anaerobic membranes.

Figure 6. Bioactivity measured in the biocake on aerobic and anaerobic membranes. Evaluation was made based on **(A)** ATP content of aerobic membranes, **(B)** ATP content of anaerobic membranes, **(C)** AI-2 content of aerobic membranes, and **(D)** AI-2 content of anaerobic membranes.

Figure 7. Ordination analysis of aerobic and anaerobic samples. **(A)** Principal component analysis of the ATP, AI-2, protein PN and carbohydrate CH contents, **(B)** non-metric multidimensional scaling plot of microbial communities.

Table 1. Operational taxonomic units (OTUs) that were increased in relative abundance with time on the **(A)** aerobic membranes, and **(B)** anaerobic membranes. OTUs were blast for their best-matched identities based on partial 16S rRNA gene sequences.

A) Aerobic membrane				
Best-matched species	**3-week Avg. (%)**	**4-week Avg. (%)**	**5-week Avg. (%)**	**Identity (%)**
Prolixibacter bellariivorans	0.52	2.68	2.14	86
Ferruginibacter lapsinanis	0.44	3.93	7.46	96
Cloacibacterium rupense	0.092	0.57	0.59	95
Meiothermus granaticius	1.13	1.88	3.90	93
Terrimonas rubra	0.84	0.88	0.86	98
Ferruginibacter lapsinanis	0.15	1.94	3.77	96
Melioribacter roseus	0.26	1.42	1.12	82
Comamonas testosteroni	0.98	2.05	1.53	98
Zoogloea resiniphila	0.17	0.49	0.48	97
Candidatus Nitrospira defluvii	0.074	0.96	1.09	94
B) Anaerobic membrane				
Best-matched species	**3-week Avg. (%)**	**6-week Avg. (%)**	**9-week Avg. (%)**	**Identity (%)**
Smithella propionica	0.27	0.57	1.22	96
Melioribacter roseus	0.77	1.16	2.89	79
Ignavibacterium album	0.20	0.20	1.31	92
Cloacibacterium hallotis	0.25	0.42	0.50	92
Melioribacter roseus	3.04	4.17	10.3	82
Methanothermobacter tenebraru	0.27	0.54	0.68	82
Oceanibaculum indicum	0.28	0.57	0.65	87
Halothiobacillus Neapolitanus	0.65	0.96	2.76	82
Melioribacter roseus	0.40	0.43	1.15	82
Cloacibacterium haliotis	0.64	0.98	1.29	96

Figure 1
Click here to download high resolution image

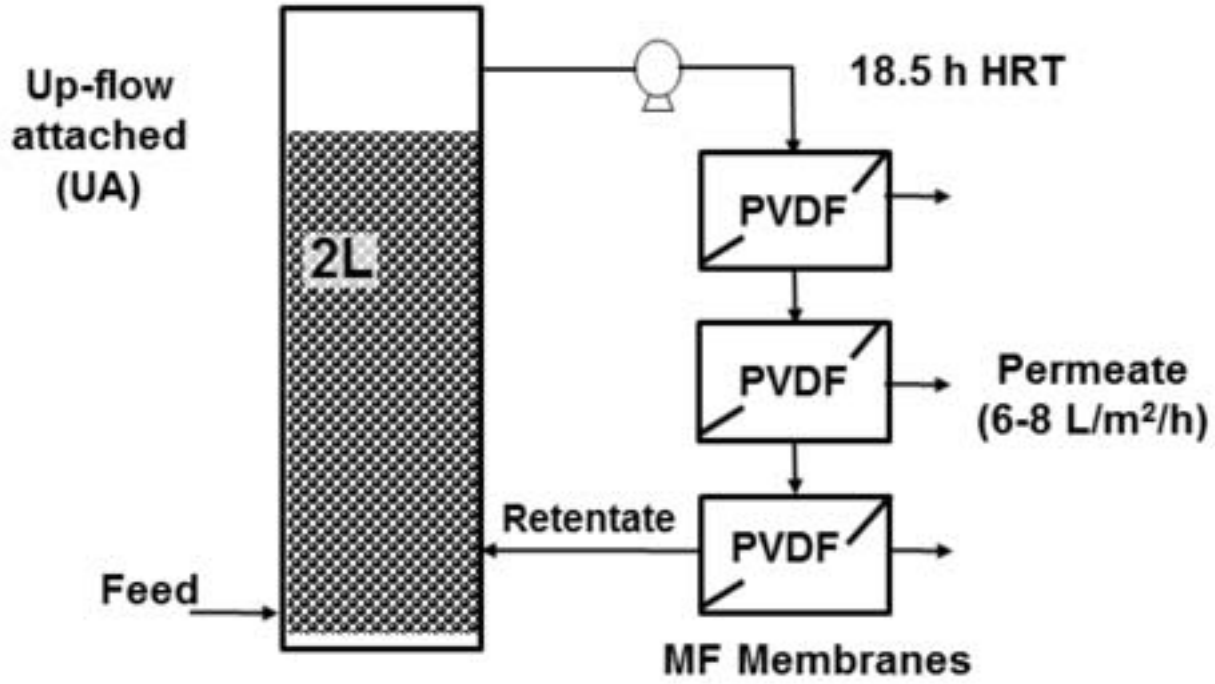

Figure 2
Click here to download high resolution image

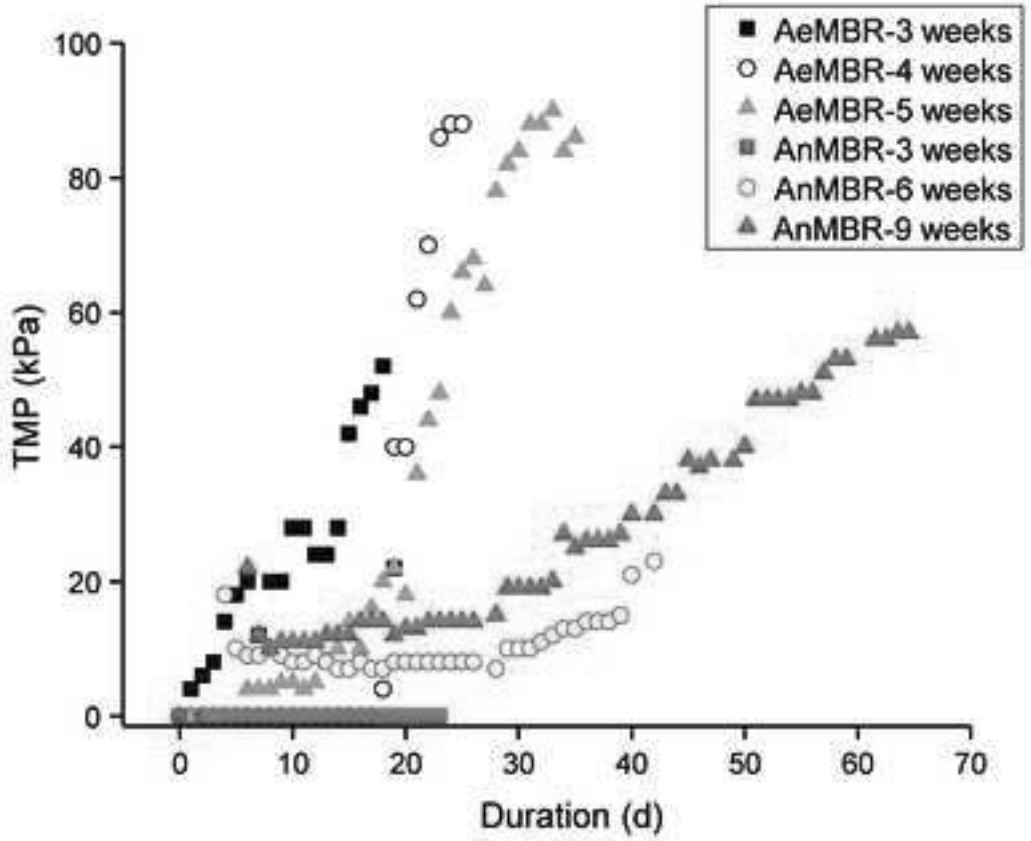

Figure 3

Click here to download high resolution image

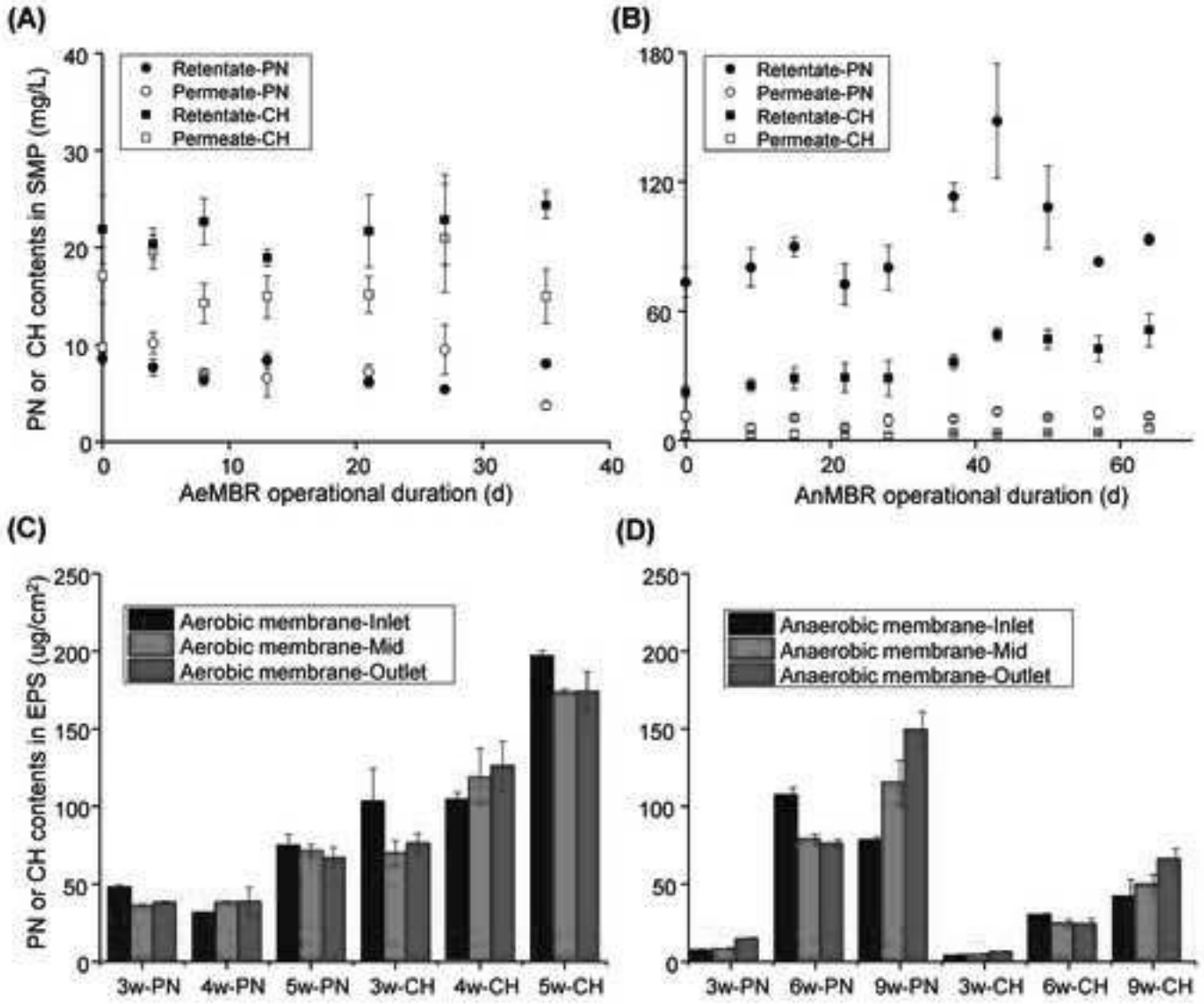

Figure 4

Click here to download high resolution image

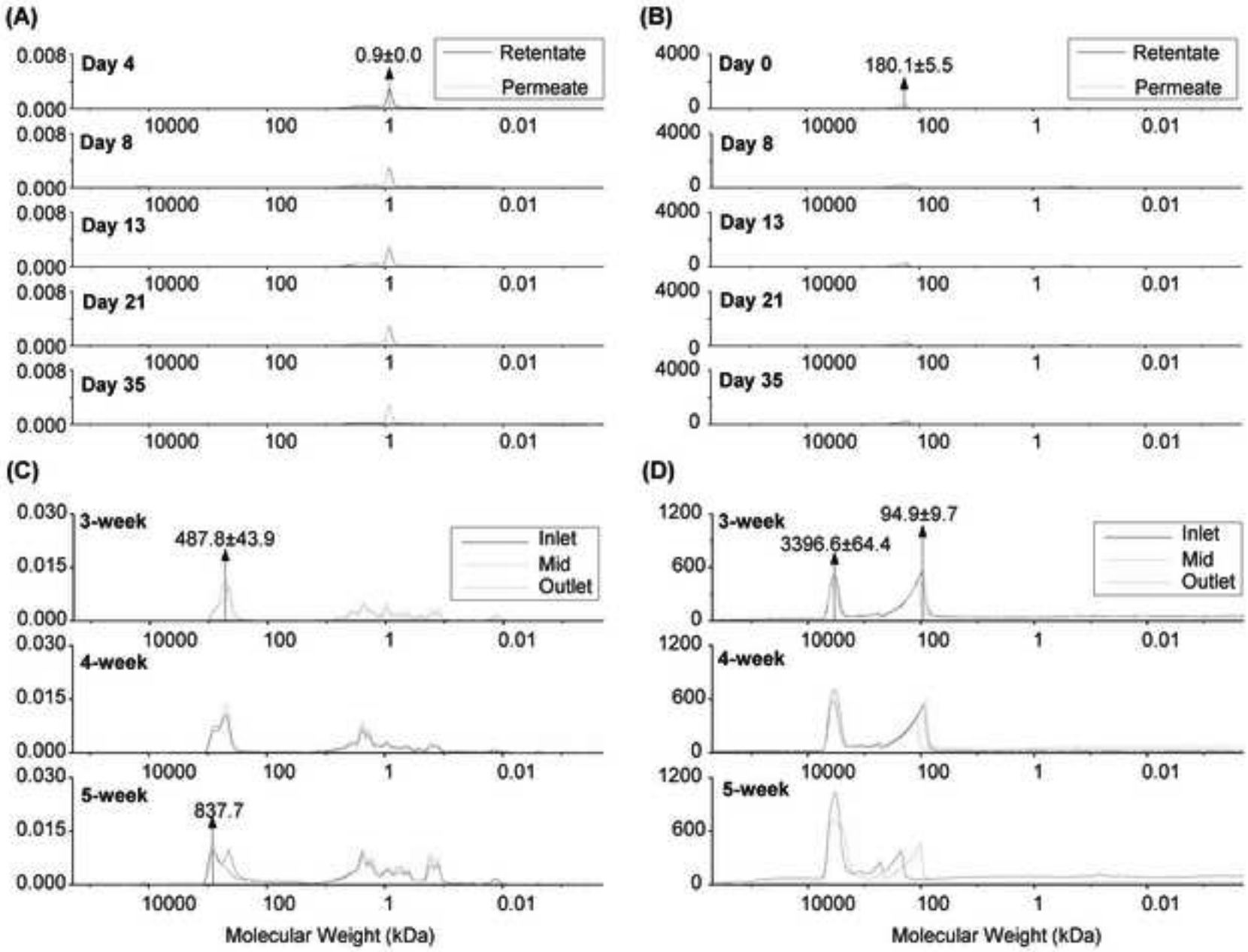

Figure 5

Click here to download high resolution image

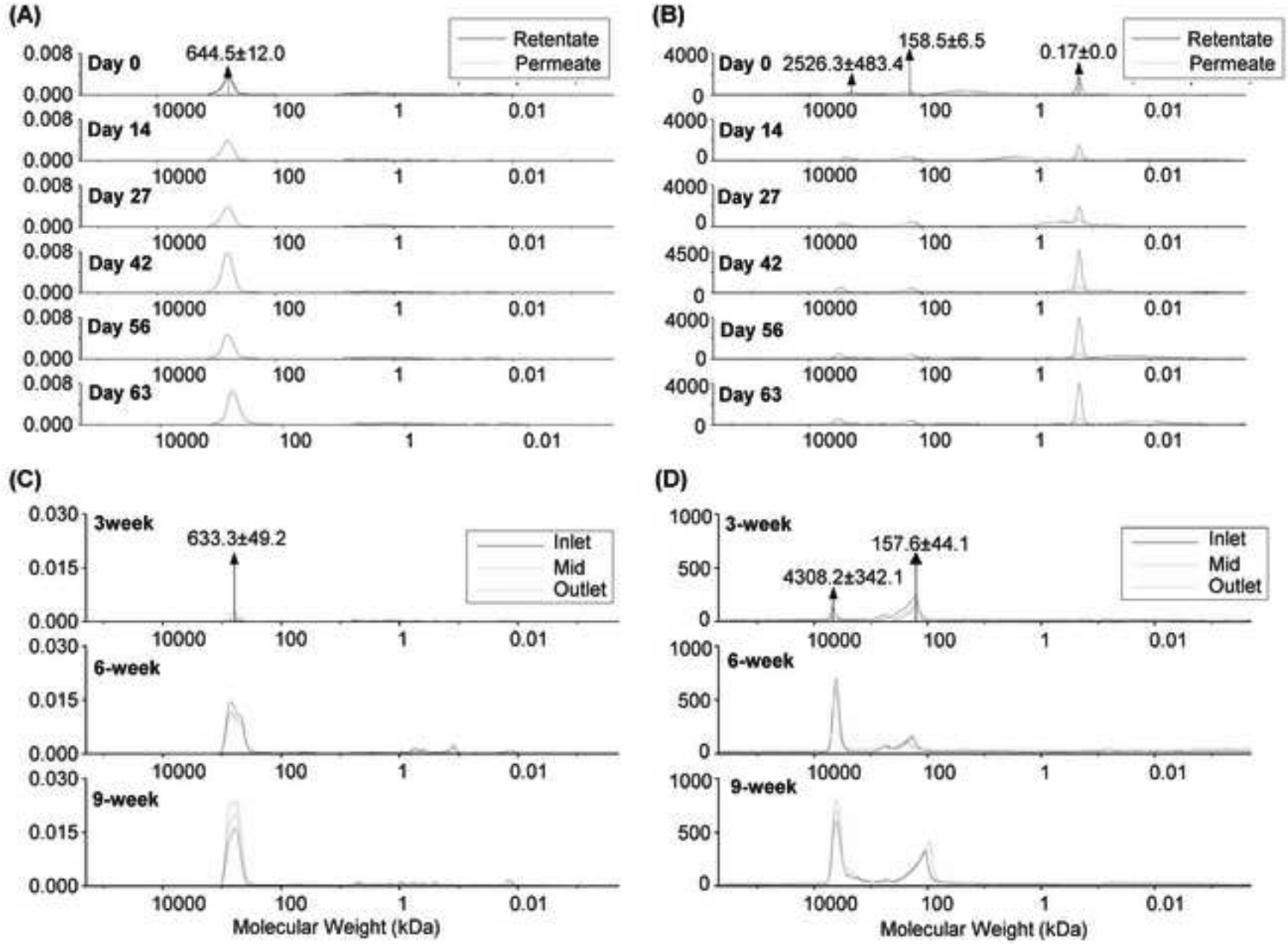

Figure 6
Click here to download high resolution image

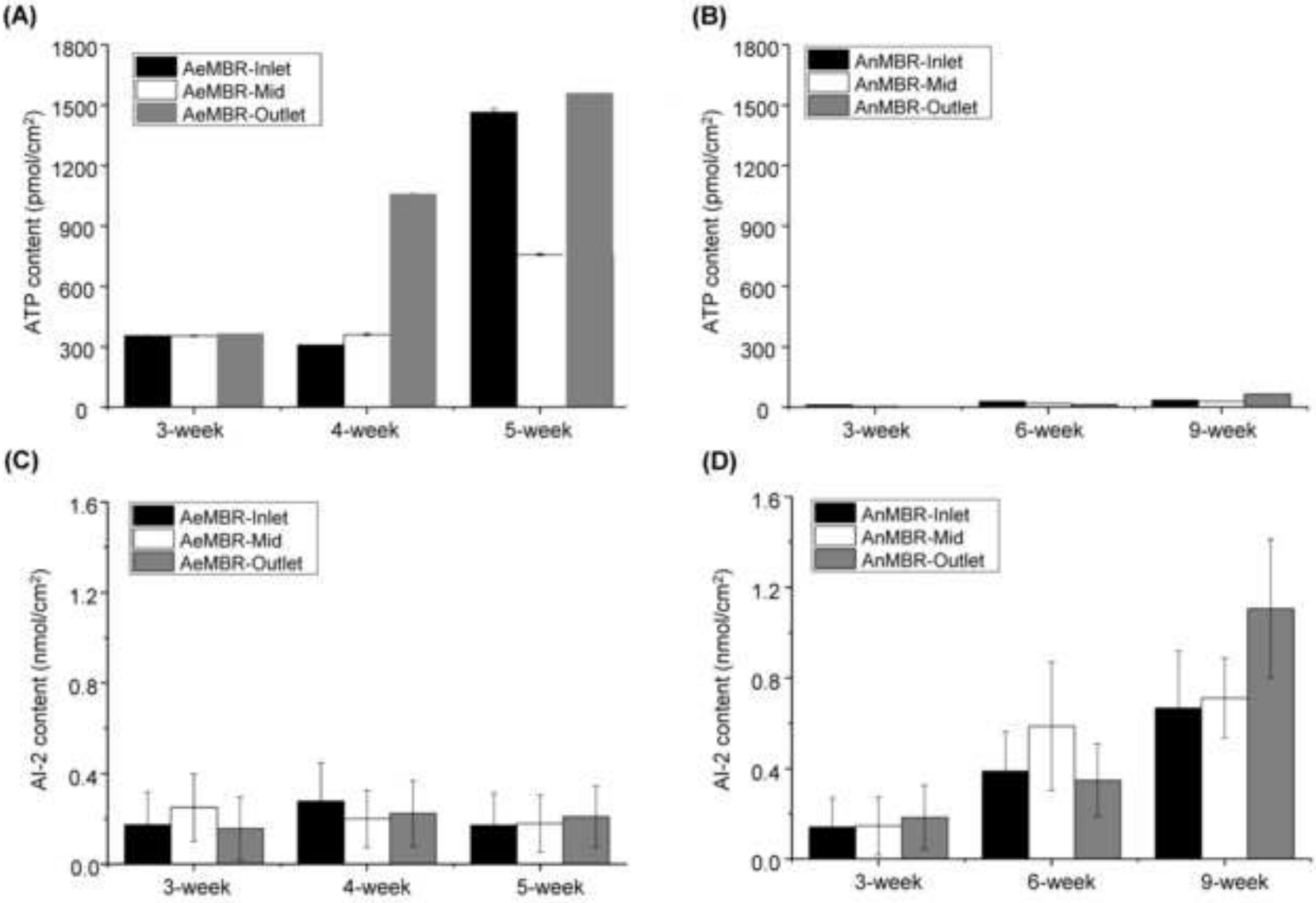

Figure 7
Click here to download high resolution image